Characteristic lengths of transmembrane peptides controlling their tilt and lateral distribution between membrane domains

Oleg V. Kondrashov,* Konstantin V. Pinigin, and Sergey A. Akimov†
A. N. Frumkin Institute of Physical Chemistry and Electrochemistry, Russian Academy of Sciences, 31/4 Leninskiy prospekt, Moscow 119071, Russia

(Received 29 January 2021; revised 8 September 2021; accepted 4 October 2021; published 22 October 2021)

Lipids and proteins of plasma membranes of eukaryotic cells are supposed to form protein-lipid domains, characterized by a different molecular order, bilayer thickness, and elastic parameters. Several mechanisms of preferable distribution of transmembrane proteins to the ordered or disordered membrane domains have been revealed. The mismatch between the length of the protein transmembrane domain and hydrophobic thickness of the lipid bilayer is considered to be an important driving force of protein lateral sorting. Utilizing the continuum theory of elasticity, we analyzed optimal configurations and preferable membrane domains for single-pass transmembrane peptides of various hydrophobic lengths and effective molecular shapes. We obtained that short transmembrane peptides stand perpendicularly to the membrane plane. The exceedance of a certain characteristic length leads to the tilt of the peptide. This length depends on the bilayer thickness. Thus, in the membrane with coexisting ordered (thicker) and disordered (thinner) phases tilting of the peptide in each phase is governed by its individual characteristic length. The lateral distribution of the peptides between ordered and disordered membrane domains is shown to be described by two additional characteristic lengths. The exceedance of the smaller one drives the peptide towards a more ordered and thicker membrane, while the exceedance of the larger characteristic length switches the preferable membrane domain from ordered and thicker to disordered and thinner. Thus, membrane proteins with long enough transmembrane domains are predicted to accumulate in the thinner disordered membrane as compared to the thicker ordered bilayer. For hourglass-like and barrel-like shaped transmembrane peptides the specific regime of sorting was obtained: the peptides distributed almost equally between the phases in a wide range of peptide lengths. This finding allowed explaining the experimental data on lateral distribution of transmembrane peptide tLAT.

DOI: 10.1103/PhysRevE.104.044411

I. INTRODUCTION

Plasma membranes of mammalian cells are laterally inhomogeneous [1,2]. Lipids and membrane proteins form domains of 10–200 nm in size [1–4]. If enriched in sphingomyelin and cholesterol, such domains are referred to as rafts [5]. Rafts provide compartmentalization of the plasma membrane as, along with a specific lipid composition, they accumulate some membrane proteins and expel the others [1,6,7]. Cells treated with mild nonionic detergent at low temperature (e.g., 4°C) followed by ultracentrifugation yield a low-density fraction enriched in sphingomyelin, cholesterol and some membrane proteins [8–10]. This relatively detergent-resistant fraction is considered to correspond to rafts of intact plasma membranes [8–10]. The detergent extraction provides an "operational" definition of raft-associated proteins. The driving forces responsible for the distribution of membrane proteins towards rafts or towards the surrounding membrane are the focus of intensive studies [6,7,11].

The small size of cellular rafts substantially complicates their study *in vivo*. However, in model lipid membranes the composition of which resembles the lipid composition of the outer leaflets of plasma membranes, micron-sized domains can be formed in the course of the phase separation induced by a temperature decrease [12–15]. Albeit with some reservations, such domains are used as models of cellular rafts. In model membranes the decrease of temperature leads to the phase separation resulting in the formation of coexisting liquid-ordered (L_o) and liquid-disordered (L_d) phases; the raft-like domains are liquid-ordered [12,15,16]. The L_o phase is enriched in saturated lipids and cholesterol [12,14]. With very rare exceptions, the domains of the L_o phase are bilayer, i.e., if there is a monolayer ordered domain in one membrane leaflet, then there will be a monolayer ordered domain in the opposite leaflet at the same position [13,15–17]. The L_o bilayer is thicker than the L_d membrane by about 0.5–1 nm [1,18–20]. Elastic moduli of the L_o phase are higher than those of the L_d phase [21,22]. If the phases were homogeneous up to the boundary, a step in the bilayer thickness would exist. Along the step, the hydrophobic membrane interior would contact with a polar medium, either water or polar lipid heads. It is assumed that elastic deformations arise at the L_o/L_d phase boundary to smooth the bilayer thickness step [23–25]. The energy of the elastic deformations related to the unit length of the interphase boundary is considered as a substantial contribution to the interphase line tension [23–25]. The line tension

*Corresponding author: academicoleg@yandex.ru
†Corresponding author: akimov_sergey@mail.ru

plays an important role in the formation of L_o domains. The kinetics of the phase separation is strongly regulated by the value of the line tension [26–29]. The free energy of the two-dimensional nucleus of the new L_o phase formed in the initially homogeneous membrane can be written as [26,29] $W = 2\pi R\gamma + \pi R^2 \Delta\mu$, where R is the L_o domain (nucleus) radius, γ is the line tension at the L_o/L_d phase boundary, and $\Delta\mu < 0$ is the difference of chemical potentials of the membrane components inside and outside the L_o domain. Such a dependence of the free energy on the domain radius means that the nucleus formation is an activation process, the height of the energy barrier of which is given by $W^* = -\pi\gamma^2/\Delta\mu = \pi\gamma^2/|\Delta\mu|$. Thus, high line tension hinders the initial stage of the phase separation, as it increases the energy barrier of the nucleus formation, and deeper quenching (lower temperature) is needed to demix the homogeneous membrane. However, at the latest stage of the phase separation (so-called Ostwald ripening [26,28,29]) the distribution of the lipid material between the domains of the newly formed L_o phase is driven by the line tension. The Laplace pressure inside of the domain of radius R is $P \sim \gamma/R$, and thus at constant γ, small domains have higher Laplace pressure as compared to large domains. This leads to lipid flow from smaller domains towards larger ones, and the average domain radius in the ensemble increases with the time t as $\langle R\rangle \sim (\gamma t)^{1/3}$ [29]. Besides, after the phase separation, the line tension favors the fusion of small domains into larger ones, as in this process the total length of the interphase boundary decreases. Thus, although the line tension hinders the initial stage of L_o/L_d phase separation, it accelerates the late stages and yields larger domains in the final equilibrium state of the membrane.

The difference in physicochemical characteristics is considered to be an important determinant of protein sorting between L_o and L_d phases [6,7,11]. Proteins can prefer a particular lipid environment; moreover, it might be crucial for proper protein functioning [30–32]. The study of mechanisms of the protein lateral sorting can be focused on two possible purposes. The first one is to adjust the membrane phase properties in order to provide the desired distribution coefficient of the particular protein between the phases. In an alternative approach, the purpose is to formulate criteria that must be met by a protein for optimal distribution between the coexisting phases of a given composition and characteristics. In the series of works [6,7,11,33,34], it was demonstrated that the distribution of transmembrane proteins between the L_o/L_d phases is determined: (1) by the length, L_p, of the transmembrane domain (TMD) (longer TMDs prefer the L_o phase); (2) by the volume of amino acids comprising the TMD (less bulky TMDs prefer the L_o phase); and (3) by the posttranslational modification (palmitoylation/miristoylation shifts the distribution towards the L_o phase). The first criterion was formulated already in early works on the role of rafts in the lateral sorting of membrane proteins in the form of the concept of a hydrophobic matching. According to this concept, the lateral distribution of transmembrane proteins between membrane phases is driven by the tendency to match the length of TMDs, L_p, with the hydrophobic thickness, $2h$, of the lipid bilayer. If the perfect matching is impossible, then the protein prefers the bilayer, the hydrophobic thickness of which has a minimal mismatch with the protein's TMD. Thus, proteins having longer TMDs should prefer the thicker L_o phase, while proteins with relatively short TMD should distribute into the thinner L_d phase.

In the framework of the concept of the hydrophobic matching, the energy gain or penalty of the distribution of the protein to a certain phase is determined by the energy of elastic deformations of the membrane arising unavoidably in the case of nonperfect matching. If the length of a cylindrically shaped TMD exactly coincides with the hydrophobic thickness of the lipid bilayer ($L_p = 2h$), no deformations arise, and the elastic energy is zero. In the case when the length of TMD and the hydrophobic thickness of lipid bilayer do not match exactly, the absence of deformations would lead to the contact of either the hydrophobic TMD with water or polar lipid heads ($L_p > 2h$) or the hydrophobic membrane interior with water or polar juxtamembrane regions of the protein ($L_p < 2h$). This unfavorable contact of the polar and hydrophobic media can be diminished at the expense of membrane deformations in the vicinity of the protein. Moreover, from theoretical estimations, it follows that elastic deformations should completely compensate for the hydrophobic mismatch, i.e., it is energetically favorable to deform the membrane to nullify the area of contact of the hydrophobic and polar media [23]. The characteristic length of the deformation decay is several nanometers [35–37]. The overlap of the deformations induced by different membrane inclusions (e.g., transmembrane proteins) may lead to their effective lateral interaction, mediated by the membrane [35–37]. Thus, in addition to driving transmembrane proteins to a certain membrane phase, hydrophobic mismatch may influence their lateral aggregation or clustering. Such deformation-mediated interactions between membrane inclusions were studied in numerous theoretical works [38–42].

The energy penalty in the case of the hydrophobic mismatch was shown to be large enough to induce the local formation of the L_o phase around relatively long TMDs even in the case of the absence of conditions for the global L_o/L_d phase separation in the membrane [43,44]. Such a local phase separation induced by an inhomogeneity (e.g., TMD) is referred to as wetting. This means that at certain conditions it is energetically favorable to form a small patch of the otherwise unstable L_o phase to facilitate compensation of the hydrophobic mismatch between the lipid bilayer and a long enough TMD. Thus, in addition to driving the lateral distribution of transmembrane proteins between coexisting membrane phases, the hydrophobic mismatch may induce the local formation of the appropriate phase around the transmembrane protein.

However, strictly speaking, the hydrophobic matching model provides obvious and physically transparent results only when the TMD is cylindrical and its length is smaller than or equal to the hydrophobic thickness of the bilayer, $L_p \leqslant 2h$. Indeed, in the case of the equality between the length and thickness ($L_p = 2h$), the optimal orientation of the protein is parallel to the membrane normal, and no elastic deformations arise around the cylindrical TMD [Fig. 1(a)]. When the TMD length is smaller than the hydrophobic thickness of the bilayer ($L_p < 2h$), the membrane in the vicinity of the protein has to compress; however, due to the symmetry, the compression deformation is isotropic, and the protein is still oriented along the membrane normal [Fig. 1(b)]. When

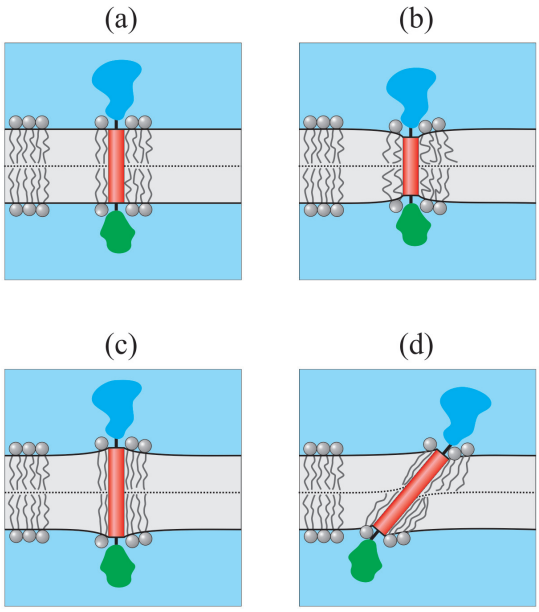

FIG. 1. Possible ways of the compensation for the hydrophobic mismatch between the length of the TMD (shown as a red rectangle) and hydrophobic thickness of the lipid bilayer (shown in a light gray). A cross section by the plane perpendicular to the membrane surface and passing through the axis of revolution of cylindrical TMD is schematically presented. (a) In the case of $L_p = 2h$ there is no mismatch; the TMD perfectly fits the bilayer, and no membrane deformations arise. (b) If $L_p < 2h$, the membrane has to compress around the TMD; the arising deformation is radially symmetric (isotropic). (c) If $L_p > 2h$, the TMD may stand vertically and induce radially symmetric (isotropic) stretching of the membrane. (d) Another possible way to compensate for the hydrophobic mismatch in the case of $L_p > 2h$ is to tilt the TMD with respect to the membrane plane, thereby breaking the rotational symmetry of the system.

the length of the TMD exceeds the hydrophobic thickness of the bilayer ($L_p > 2h$), the protein can stand along the membrane normal and isotropically stretch the membrane in its vicinity [Fig. 1(c)]. Alternatively, the protein can break the symmetry and tilt with respect to the membrane normal to completely hide its TMD in the hydrophobic core of the bilayer [Fig. 1(d)]. This should obviously occur when the TMD length substantially exceeds the hydrophobic thickness of the lipid bilayer. Indeed, according to Hooke's law, the energy of isotropic stretching of the membrane induced by the vertical TMD is proportional to the square of the hydrophobic mismatch, i.e., to $(L_p–2h)^2$, while the elastic energy induced by the tilted TMD should grow linearly in L_p. Thus, in the case of a relatively long TMD the prediction of the hydrophobic matching model is not straightforward. The situation is even more complex, as the elastic moduli of the L_o bilayer are higher than those of the L_d membrane [21,22], and formally a smaller deformation induced by a long TMD in the thicker L_o bilayer may nevertheless cost a larger amount of energy as compared to the thinner but softer L_d membrane. Besides, the effective shape of a typical TMD is generally expected to deviate from the cylindrical towards an hourglass-like one, as charged and/or aromatic amino acid residues responsible for a proper TMD positioning with respect to polar or hydrophobic boundaries of the membrane [45–47] are relatively bulky. The noncylindrical shape of the TMD should give rise to elastic deformations even in the case of the perfect matching between the TMD length and hydrophobic thickness of the bilayer. Thus, the energy landscape of protein configurations requires a detailed investigation.

In the present work, we utilize the theory of elasticity of lipid membranes to obtain optimal configurations of cylindrically, hourglass-like and barrel-like shaped TMDs in lipid bilayers characterized by different hydrophobic thicknesses and elastic moduli. Cases of both isotropic and anisotropic deformations were considered. We show that the landscape of optimal configurations of transmembrane proteins in the membrane with coexisting L_o and L_d phases is characterized by several characteristic lengths of TMDs. In the optimal configuration, relatively short TMDs stand perpendicular to the membrane plane and induce radially symmetric (isotropic) deformations. When the first characteristic length, L_1, is exceeded, the isotropic optimal orientation of the proteins in the L_d bilayer switches to the tilted one, i.e., the configuration illustrated in Fig. 1(c) switches to the configuration of Fig. 1(d). The TMDs, the length of which exceeds the second characteristic length L_2, are driven from the L_d bilayer to the L_o phase, as the associated elastic energy becomes higher in the L_d membrane as compared to the L_o phase due to the larger hydrophobic thickness of the L_o bilayer. The third characteristic length, L_3, corresponds to the switching of the isotropic orientation of the protein in the L_o bilayer to the tilted one. Finally, when the fourth characteristic length, L_4, is exceeded, the energy of the protein-induced elastic deformations in the L_o phase becomes higher than the energy of the deformations the protein would induce in the L_d bilayer. This leads to a quite counterintuitive prediction: proteins with long enough TMDs should prefer to accumulate in the thinner (but softer) L_d membrane rather than in the thicker (but more rigid) L_o bilayer. Such a pattern is modulated by the degree of the deviation of the TMD shape from the cylindrical one and the value of the spontaneous curvature of lipid monolayers.

II. MODELS AND METHODS

We describe elastic deformations of the membrane within the framework of the continuum theory of elasticity originally developed by Hamm and Kozlov [48]. The approximation of the continuous medium is justified since the characteristic lengths of membrane deformations are substantially larger than the lateral size of lipid molecules. We introduce a Cartesian coordinate system $Oxyz$ in such a way that the intermonolayer surface of the flat unperturbed membrane coincides with the Oxy plane (Fig. 2). For definiteness, the membrane plane is assumed to be horizontal; the lipid monolayer lying in the half-space $z > 0$ is referred to as upper, while the opposing monolayer is lower. The functions, variables and parameters related to the upper monolayer are denoted by index u, to the bottom by index l. The center of the transmembrane domain (peptide) is placed at the point $x = y = z = 0$ (Fig. 2). The TMD is assumed to be tilted in the Oxz plane. The orientation of the TMD is characterized by the lateral shift, l, of its upper edge center in the direction of the Ox axis (Fig. 2). The tilted TMD reorients its adjacent

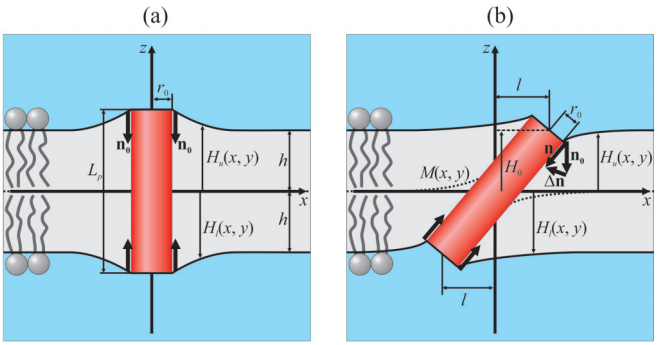

FIG. 2. Illustration of parameters defining configurations of the membrane with the incorporated vertical (a) or tilted (b) transmembrane domain. The cross section of the system by the plane passing through the axis of revolution of the TMD is schematically shown. See text for details.

lipids; the tilt is also followed by displacements of the neutral surfaces of the upper and lower monolayers (Fig. 2).

An average orientation of lipid hydrophobic chains is described by a vector field of unit vectors called directors, $\mathbf{n}$. This field is defined at the neutral surface, which lies inside the monolayer at the region of the junction of polar heads and hydrophobic chains of lipid molecules [49]. The shape of the neutral surface is characterized by the field of its unit normal vectors, $\mathbf{N}$, and by the z-coordinate of the surface, $H(x, y)$, in the introduced Cartesian coordinate system (Fig. 2). All deformations are deemed small, and their energy is considered in the quadratic order. We account for the following deformations of the lipid monolayer: (1) bending, the energy (per unit area of the neutral surface) of which is given by $\frac{B}{2}[\mathrm{div}(\mathbf{n}) + J_0]^2 - \frac{B}{2}J_0^2$; B, J_0 are the bending modulus and spontaneous curvature of the monolayer, respectively; (2) tilt, the energy surface density of which is given by $\frac{K_t}{2}\mathbf{t}^2$, where K_t is the tilt modulus and $\mathbf{t} = \mathbf{n}/(\mathbf{nN})$–$\mathbf{N} \approx \mathbf{n}$–$\mathbf{N}$ is the tilt vector; (3) lateral stretching, the energy surface density of which is given by $\frac{K_a}{2}\alpha^2$, where K_a is the modulus of the lateral stretching and $a = (a–a_0)/a_0$ is the relative change of the area per lipid molecule, a, with respect to the initial area, and a_0, at the neutral surface; (4) lateral tension of the monolayer, the energy surface density of which is given by $\frac{\sigma}{2}[\mathbf{grad}(H)]^2$, where σ is the monolayer lateral tension; (5) Gaussian curvature, the energy surface density of which is given by $K_G K$, where K_G, K are the Gaussian curvature modulus and Gaussian curvature, respectively; and (6) twist, the surface energy density of which is given by $\frac{K_{\mathrm{rot}}}{2}[\mathbf{rot}(\mathbf{n})]^2$, where K_{rot} is the twist modulus; for unidimensional or axially symmetric configurations, as well as for the case of $\mathbf{t} \equiv \mathbf{0}$, this contribution is absent [50].

The ground state of the membrane is considered flat. The deformation energy of the lipid monolayer can be written as [35,38,41,51]

$$W = \int dS \left\{ \frac{B}{2}[\mathrm{div}(\mathbf{n}) + J_0]^2 - \frac{B}{2}J_0^2 + \frac{K_t}{2}\mathbf{t}^2 + \frac{\sigma}{2}[\mathbf{grad}(H)]^2 + \frac{K_a}{2}\alpha^2 + K_G K + \frac{K_{\mathrm{rot}}}{2}[\mathbf{rot}(\mathbf{n})]^2 \right\}, \quad (1)$$

where the integration is carried out over the neutral surface of the monolayer. The deviations of all deformation fields from the state of the flat membrane are considered small. The director field, in particular, is expressed as $\mathbf{n}_{u,l} = [n_x(x, y), n_y(x, y), \mp 1]^T$, where "–" corresponds to the upper, and "+" to the lower monolayer; T is the transposition.

We also assume that the lipid monolayer is locally volumetrically incompressible, i.e., that each element of the monolayer preserves its original volume upon deformations. This assumption is justified by large values of the bulk modulus of lipid membranes ($\sim 10^{10}\,\mathrm{J/m^3} \approx 3 \times 10^3 k_B T/\mathrm{nm^3}$ [52]; here $k_B T \approx 4.14 \times 10^{-21}$ J). The local incompressibility imposes restrictions on possible deformations. Within the required accuracy, one can write for the upper and lower monolayers, respectively [35,38,41,48,51]:

$$H_u - M = h - \frac{h^2}{2}\mathrm{div}(\mathbf{n}_u) - h\alpha_u,$$
$$M - H_l = h - \frac{h^2}{2}\mathrm{div}(\mathbf{n}_l) - h\alpha_l, \quad (2)$$

where $M(x, y)$ is the z-coordinate of the monolayer interface (Fig. 2). Within the required accuracy, the unit normal vectors to the neutral surfaces of the upper and lower monolayers can be written as $\mathbf{N}_{u,l} = (\pm\partial H_{u,l}/\partial x, \pm\partial H_{u,l}/\partial y, \mp 1)^T = \pm\mathbf{grad}(H_{u,l})$, where the upper signs correspond to the upper and the lower to the lower monolayer. Thus, the tilt vector can be expressed as $\mathbf{t}_{u,l} = \mathbf{n}_{u,l} - \mathbf{N}_{u,l} = \mathbf{n}_{u,l} \mp \mathbf{grad}(H_{u,l})$. We express $\alpha_{u,l}$ from Eqs. (2), substitute it into the elastic energy functional, Eq. (1), along with the expression for the tilt vector, and obtain

$$\begin{aligned} W = \int dS_u \Big\{ & \frac{B}{2}[\mathrm{div}(\mathbf{n}_u) + J_0]^2 - \frac{B}{2}J_0^2 \\ & + \frac{K_t}{2}[\mathbf{n}_u - \mathbf{grad}(H_u)]^2 + \frac{\sigma}{2}[\mathbf{grad}\,(H_u)]^2 \\ & + \frac{K_a}{2h^2}\left[h - \frac{h^2}{2}\mathrm{div}(\mathbf{n}_u) + M - H_u\right]^2 \\ & + K_G K_u + \frac{K_{\mathrm{rot}}}{2}[\mathbf{rot}(\mathbf{n}_u)]^2 \Big\} \\ & + \int dS_l \Big\{ \frac{B}{2}[\mathrm{div}(\mathbf{n}_l) + J_0]^2 - \frac{B}{2}J_0^2 \\ & + \frac{K_t}{2}[\mathbf{n}_l + \mathbf{grad}(H_l)]^2 + \frac{\sigma}{2}[\mathbf{grad}\,(H_l)]^2 \\ & + \frac{K_a}{2h^2}\left[h - \frac{h^2}{2}\mathrm{div}(\mathbf{n}_l) - M + H_l\right]^2 \\ & + K_G K_l + \frac{K_{\mathrm{rot}}}{2}[\mathbf{rot}(\mathbf{n}_l)]^2 \Big\}. \end{aligned} \quad (3)$$

The energy functional Eq. (3) should be supplemented by specific boundary conditions in the vicinity of the membrane inclusion (the TMD incorporated into the membrane), as well as by general conditions at infinity (far from the inclusion):

$$\begin{aligned} \mathbf{n}_{u,l}(\infty) &= (0, 0, \mp 1), \\ M(\infty) &= 0, \\ H_u(\infty) &= h, \\ H_l(\infty) &= -h. \end{aligned} \quad (4)$$

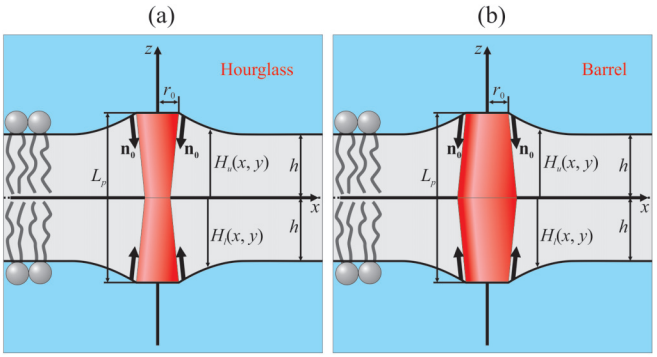

FIG. 3. Schematic representation of hourglass-like (a) and barrel-like (b) shaped TMDs. The cross section of the system by the plane passing through the axis of revolution of the TMDs is schematically shown.

For vertically inserted cylindrical TMDs, the following specific boundary conditions are used:

$$\begin{aligned} &\mathbf{n}_u(r=r_0)=\mathbf{0},\\ &\mathbf{n}_l(r=r_0)=\mathbf{0},\\ &H_u(r=r_0)-H_l(r=r_0)=L_p, \end{aligned} \tag{5}$$

where $\mathbf{n}_u$ and $\mathbf{n}_l$ are the corresponding directors of the upper and lower monolayers at the peptide boundary, r is the radial coordinate in the polar coordinate system, the center of which is located at the center of the TMD edge, r_0 is the peptide radius, and L_p is the length of the TMD. It should be noted that vertically inserted cylindrical TMDs do not deform the membrane if their hydrophobic length coincides with the hydrophobic thickness of the lipid bilayer, $L_p = 2h$.

To analyze the influence of spontaneous curvatures of L_o and L_d phase monolayers, we also consider the cases of hourglass-like [Fig. 3(a)] and barrel-like [Fig. 3(b)] (i.e., noncylindrical) shapes of the TMDs. For simplicity, only symmetric with respect to the membrane midplane shapes of the TMDs are considered.

Let us denote normal and tangential components of the boundary director as n_n and n_t, respectively. Then the conditions at the boundary of the hourglass-like or barrel-like TMD with the vertical axis of revolution (directed along Oz axis) can be written as

$$\begin{aligned} &n_n^{u,l}(r=r_0)=n_{n0},\\ &n_t^{u,l}(r=r_0)=0,\\ &H_u(r=r_0)-H_l(r=r_0)=L_p; \end{aligned} \tag{6}$$

$n_{n0} < 0$ corresponds to the hourglass-like TMD, while $n_{n0} > 0$ corresponds to barrel-like TMD.

In the case of a tilted TMD, the boundary conditions are modified. It should be taken into account that when the TMD is tilted, the boundary conditions are set at different points (x, y) for the upper and lower monolayers. For the upper monolayer, the boundary conditions are set on a circle of radius r_0 and center coordinates (l, H_0) (boundary Γ_u), and for the lower monolayer on a circle of radius r_0 and center coordinates $(-l, -H_0)$ (boundary Γ_l) [see Fig. 2(b)]. We denote the radius-vector of the points of either boundary as $\mathbf{r} = (x, y)^T$. Upon tilting of the TMD, the tilt vector value $\Delta\mathbf{n}$ is added to the boundary director, $\mathbf{n}_0(\mathbf{r})$, of the symmetric configuration with the vertical axis of revolution; the resulting boundary director in the tilted configuration becomes equal to $\mathbf{n}_0(\mathbf{r}) + \Delta\mathbf{n}$ [Fig. 2(b)]. For TMD rotating in the membrane clockwise in the Oxz plane, the components of the tilt vector in the upper monolayer can be written as

$$\Delta n_{ux} = -\frac{2l}{L_p}, \quad \Delta n_{uy} = 0, \tag{7}$$

where l is the x-coordinate of the center of the upper edge of the TMD [Fig. 2(b)]. In the case of the tilted TMD, the third boundary condition in Eqs. (5) and (6) changes similarly with the substitution:

$$H_u(\mathbf{r}) = H_0 + \mathbf{r}\Delta\mathbf{n}_u, \tag{8}$$

which implies that the neutral surface of the lipid monolayer "follows" the boundary of the TMD upper edge when it is tilted; H_0 is the z-coordinate of the center of the upper edge of the TMD. To summarize, the boundary conditions can be written as

$$\begin{aligned} &\Delta n_{ux}(\Gamma_u) = -\frac{2l}{L_p}, \quad \Delta n_{uy}(\Gamma_u) = 0,\\ &\Delta n_{lx}(\Gamma_l) = \frac{2l}{L_p}, \quad \Delta n_{ly}(\Gamma_l) = 0,\\ &H_u(\Gamma_u) = H_{\text{average}} + \frac{\sqrt{L_p^2-(2l)^2}}{2} + \Delta\mathbf{r}_u\Delta\mathbf{n}_u,\\ &-H_l(\Gamma_l) = -H_{\text{average}} + \frac{\sqrt{L_p^2-(2l)^2}}{2} + \Delta\mathbf{r}_l\Delta\mathbf{n}_l,\\ &\Delta\mathbf{n}_u = \left(-\frac{2l}{L_p}, 0\right), \quad \Delta\mathbf{n}_l = \left(\frac{2l}{L_p}, 0\right). \end{aligned} \tag{9}$$

Here $\Delta\mathbf{r} = \mathbf{r}–\mathbf{r}_0$, where $\mathbf{r}$ is the radius vector of the point at the circle Γ, $\mathbf{r}_0$ is the radius vector of the center of the circle Γ. The value of H_{average} is introduced for convenience; the energy is minimized over this variable.

From the energy functional Eq. (3) it follows that within the required accuracy the energy contribution of the monolayer spontaneous curvature J_0 can be expressed explicitly as

$$W_{\text{spont}} = \int dS\{BJ_0\text{div}(\mathbf{n})\} = -BJ_0 \oint (\mathbf{n}\cdot\mathbf{a})d\Gamma, \tag{10}$$

where the last integration is performed over the TMD boundary contour Γ at the monolayer neutral surface; $\mathbf{a}$ is the outer unit normal vector to the contour. From this expression, it follows that for cylindrically shaped TMDs the elastic energy is independent on the monolayer spontaneous curvature, as in this case $\mathbf{n} \perp \mathbf{a}$ at the boundary contour, and thus $(\mathbf{n}\cdot\mathbf{a}) \equiv 0$. For hourglass-like or barrel-like shapes of TMDs with a fixed normal component of the boundary director, the corresponding contribution is a nonzero constant proportional to the monolayer spontaneous curvature but independent on the tilt angle of the TMD.

As the configuration of the tilted TMD lacks the rotational symmetry, the minimization of the energy functional Eq. (3) under the boundary conditions Eq. (4), (9) was car-

ried out numerically for a discrete set of fixed orientations of the TMD. This allowed us to obtain the dependences of the elastic energy of the membrane on l. We used the finite element method with an adaptive mesh, similar to works [35,38,41,51]. Briefly, the plane Oxy was divided into elementary triangles. In each triangle, the deformation fields were approximated by polynomials of the first degree in coordinates. Thus, smooth deformations were replaced by their first-order interpolants, set on the nodes of the computational mesh. Further, we integrated the energy surface density in Eq. (3) over the area of each elementary triangle and took the sum over all triangular regions (i.e., over the whole neutral surface) of the lipid monolayer. This yielded the approximate elastic energy of the monolayer as a function of unknown values of deformation fields at mesh nodes. The total elastic energy of the membrane W_{total} was obtained as a sum of the elastic energies of its constituent monolayers. To get the numerical value of the total elastic energy, the function W_{total} was minimized over the values of deformation fields at mesh nodes, except for those set by the boundary conditions Eq. (4), (9). The boundary conditions at $r = \infty$ were actually set at a rectangle, the sides of which were at least 25 nm far from the TMD. The distance of 25 nm substantially exceeds the characteristic lengths of decay of membrane deformations, which are typically about several nanometers [35–37]. To improve the accuracy of the approximate energy calculation, we used inhomogeneous meshes: the surface density of nodes increased in the TMD vicinity. The upper and lower boundaries of the TMD were represented in a piecewise linear approximation. The neutral surfaces of lipid monolayers around the TMD were subdivided into five regions. Each region was specified by the inequality $r_{i-1} \leqslant d \leqslant r_i$, where d is the distance to the boundary of the TMD; r_{i-1}, r_i are constants defining the inner and outer boundaries of the regions, respectively, for $i = 1, 2, 3, 4, 5$. The numerical values of r_i were $r_0 = 0$, $r_1 = 1\,\text{nm}$, $r_2 = 1.5\,\text{nm}$, $r_3 = 4\,\text{nm}$, $r_4 = 11\,\text{nm}$, $r_5 = \infty$. We restricted the maximum area of an elementary triangle of the computational mesh by 0.5γ (in nm^2), and divided the regions defined above into elementary triangles of the area not exceeding $\gamma\vartheta_i$, where $\theta_1 = 0.01$, $\theta_2 = 0.02$, $\theta_3 = 0.04$, $\theta_4 = 0.05$, $\theta_5 = 0.5$. This algorithm allowed obtaining the numerical value of W_{total} for each numerical value of γ set manually. We explicitly checked that the effect of the finiteness of the mesh size, γ, was insignificant. In several configurations of the TMD, we calculated W_{total} on five gradually decreasing meshes and extrapolated the results obtained to zero size of the mesh, $\gamma \to 0$, using second-order polynomial approximation. The following values of γ were used: 0.62, 0.85, 1.05, 1.25, 1.5. We obtained that the relative magnitude of the error of the W_{total} determination on the meshes $\gamma = 1.5$ and $\gamma \to 0$ was about 1.5% or less (Fig. 4). Thus, it appeared permissible to use the most coarse computational mesh $\gamma = 1.5$ without extrapolation to an infinitely fine mesh.

To obtain numerical results, we utilized the elastic parameters of the L_d lipid monolayer, which are similar to those of dioleoylphosphatidylcholine (DOPC): $B = 10\,k_BT$ [53], $K_t = 40\,\text{mN/m} \approx 10k_BT/\text{nm}^2$ [48], $K_a = 133\,\text{mN/m} \approx 32k_BT/\text{nm}^2$ [53], $h = 1.5\,\text{nm}$ [53], $\sigma = 0.1\,\text{mN/m} \approx 0.025\,k_BT/\text{nm}^2$, $K_G = -B/2 = -5k_BT$

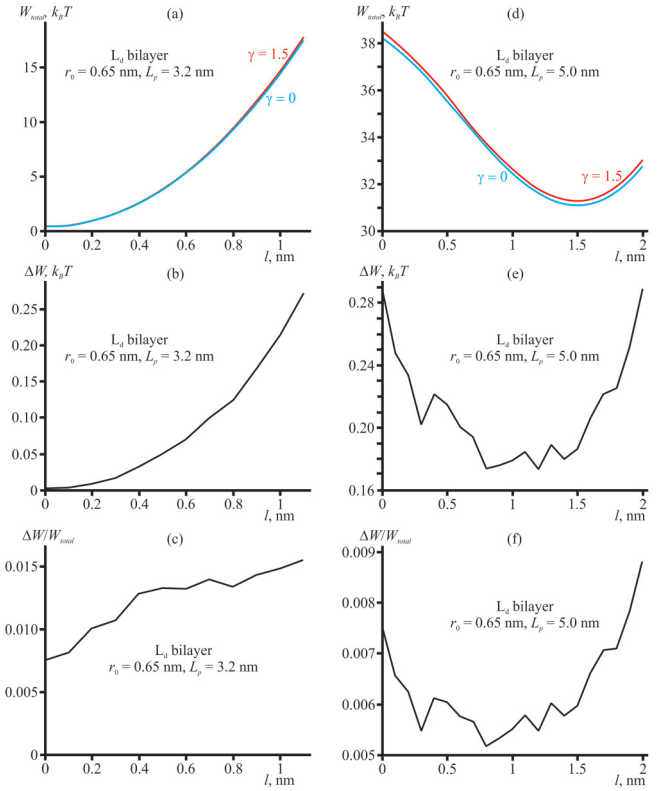

FIG. 4. The difference of elastic energies W_{total} calculated on the meshes of size $\gamma = 1.5$ and $\gamma \to 0$ is relatively small. (a)–(c) The case of the TMD of the length $L_p = 3.2\,\text{nm}$, radius $r_0 = 0.65\,\text{nm}$ incorporated into the L_d bilayer; (d)–(f) the case of the TMD of the length $L_p = 5.0\,\text{nm}$, radius $r_0 = 0.65\,\text{nm}$ incorporated into the L_d bilayer. (a), (d) The dependences of W_{total} calculated on meshes of size $\gamma = 1.5$ (red curves) and $\gamma \to 0$ (blue curves) on the lateral shift of the TMD upper edge center l. (b), (e) The differences of the red and blue curves of panels (a) and (d), respectively. (c), (f) The relative differences of the red and blue curves of panels (a) and (d), respectively.

[54], and $K_{\text{rot}} = B/2 = 5\,k_BT$ [35,41]. For the monolayer of the L_o phase we used the following parameters: $K_t = 40\,\text{mN/m} \approx 10\,k_BT/\text{nm}^2$ [48], $\sigma = 0.1\,\text{mN/m} \approx 0.025\,k_BT/\text{nm}^2$, and hydrophobic thickness $h_o = 1.8\,\text{nm}$ [55,56]. The bending modulus of L_o monolayers has been estimated to be two to five times higher than the bending modulus of L_d monolayers [21]. The modulus of the lateral stretching of the L_o phase is not actually known; it is only expected to be several times higher than that of the L_d phase [53]. Thus, in order to analyze the energy landscape of TMD configurations in the L_o phase, we used several sets of the elastic parameters: (1) "regular" L_o monolayer (denoted by index r): $B_r = 5B = 50\,k_BT$, $K_a^r = 5K_a = 160\,k_BT/\text{nm}^2$; (2) "soft-bending" L_o monolayer (denoted by index b): $B_b = 2B = 20\,k_BT$, $K_a^b = 5K_a = 160\,k_BT/\text{nm}^2$; (3) "soft bending and stretching" L_o monolayer (denoted by index a): $B_a = 2B = 20\,k_BT$, $K_a^a = K_a = 32\,k_BT/\text{nm}^2$; (4) "very soft" L_o monolayer (denoted by index e): $B_e = B = 10\,k_BT$, $K_a{}^e = K_a = 32\,k_BT/\text{nm}^2$; and (5) "firm" L_o monolayer (denoted by index f): $B_f = 5B = 50\,k_BT$, $K_a^f = 10K_a = 320\,k_BT/\text{nm}^2$. The Gaussian and twist moduli

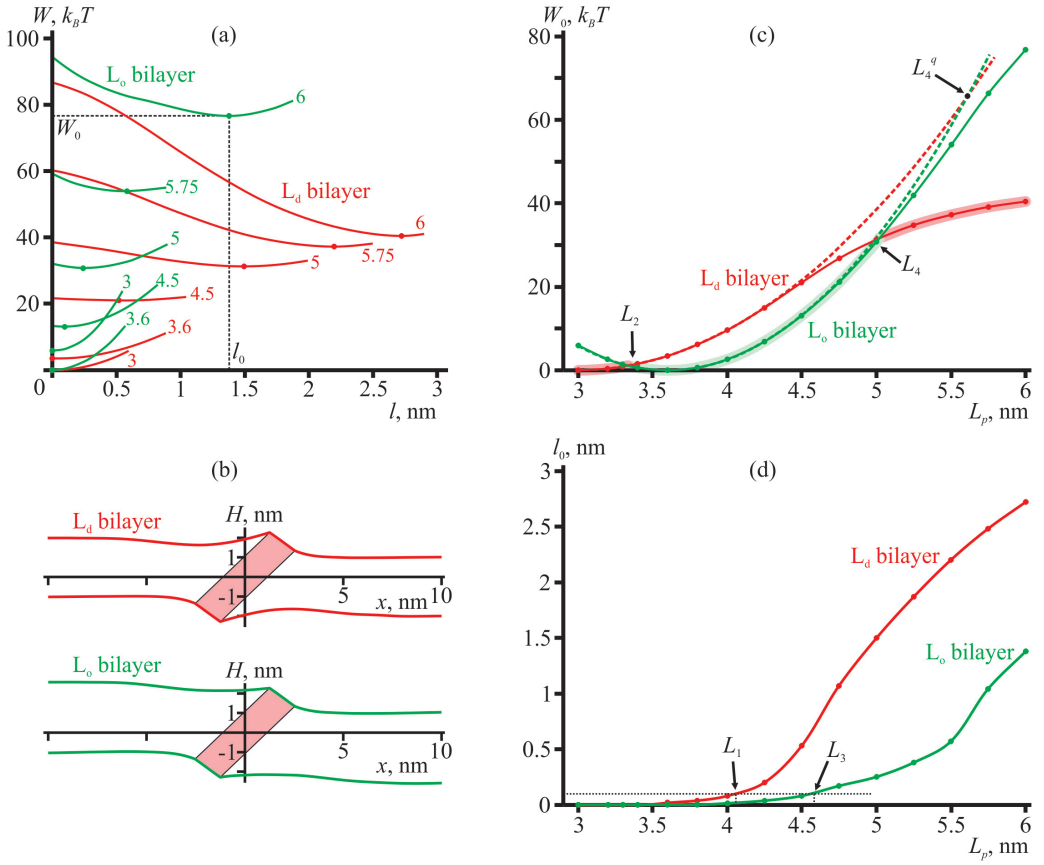

FIG. 5. The characteristic lengths of the cylindrical TMD controlling its tilt and lateral distribution between L_d and L_o phases. (a) The dependences of membrane elastic energy on the lateral shift of the TMD upper edge center for different TMD lengths (indicated near each curve, in nanometers). Red curves correspond to the TMD in the L_d bilayer, green curves in the regular L_o bilayer. Each curve has a global minimum W_0 at the optimal shift l_0; the minima are indicated by circles. (b) The shape of the membrane with the incorporated cylindrical TMD of length $L_p = 5.25$ nm tilted by $l = 1.9$ nm in the L_d bilayer (top) and regular L_o bilayer (bottom). (c) The dependence of the membrane elastic energy in configurations of optimally tilted cylindrical TMDs, W_0, on the TMD length, L_p, in the L_d bilayer (solid red curve), and regular L_o bilayer (solid green curve). The curves intersect at two characteristic lengths L_2, L_4. Dashed curves illustrate the analogous dependences for the fixed zero tilt of the TMD ($l = 0$). Wide pink and light green stripes indicate the membrane phase of the lowest energy. (d) The dependence of the optimal lateral shift of the TMD upper edge center on the TMD length. The dotted horizontal line corresponds to $l_0 = 0.1$ nm, which is arbitrarily chosen to represent a minimal substantial tilt. The intersections of the dotted line with the dependences $l_0(L_p)$ yield the characteristic lengths of the TMD tilting: $L_1 \approx 4$nm, $L_2 \approx 4.6$ nm in L_d and L_o bilayers, respectively.

of the L_o monolayer are obtained as $K_G^i = -B_i/2$, $K_{rot}^i = B_i/2$, for $i = r, b, a, e, f$. For the spontaneous curvatures of L_o and L_d monolayers we utilized either zero values ($J_0^r = J_0^s = 0$) or the values estimated from the molecular dynamics data [57]: $J_0^r = +0.1\,\text{nm}^{-1}$, $J_0^s = -0.15\,\text{nm}^{-1}$. In order to analyze possible effects of the TMD diameter, we considered two cases: $r_0 = 0.65$ nm (approximately corresponding to the radius of α-helix) and $r_0 = 1$ nm. The TMD lengths were $L_p =$ {3.0, 3.2, 3.3, 3.4, 3.6, 3.8, 4.0, 4.25, 4.5, 4.75, 5.0, 5.25, 5.5, 5.75, 6.0}nm for cylindrical TMDs, and $L_p =$ {2.75, 3.00, 3.25, 3.50, 4.00, 4.25, 4.50, 4.75, 5.00, 5.25, 5.50}nm for hourglass-like and barrel-like shaped TMDs. The length $L_p = 3.0\,\text{nm} = 2h$ fits the hydrophobic thickness of the L_d bilayer; the TMD length $L_p = 3.6$ nm $= 2h_o$ fits the hydrophobic thickness of the L_o bilayer.

III. RESULTS

A. Characteristic lengths of TMDs

First, we consider cylindrical TMDs of the radius $r_0 = 0.65$ nm, incorporated into the L_d bilayer or regular L_o bilayer. For each length L_p of the TMD, we sequentially fixed the shift l of the TMD upper edge center, starting from $l = 0$ with the step of 0.1 nm, and obtained the elastic energy W of each configuration. The dependence $W(l)$ is shown in Fig. 5(a) for several values of L_p (indicated near each curve).

Typical shapes of the membrane with the incorporated and tilted TMD are presented in Fig. 5(b), for L_d (top) and regular L_o (bottom) bilayers, respectively; the particular configuration of $l = 1.9$ nm for the TMD of the length $L_p = 5.25$ nm is illustrated. Each curve $W(l)$ in Fig. 5(a) has a global minimum

W_0 at some value of $l = l_0$. We obtain the dependences of the optimal energies on the TMD length, $W_0(L_p)$; the dependences are illustrated in Fig. 5(c). The optimal values l_0 for each L_p are shown in Fig. 5(d). From the plots it follows that relatively short cylindrical TMDs of lengths in the range of 3 to 3.4 nm prefer to stand vertically ($l_0 = 0$) in the L_d phase, as the elastic energy of the membrane in this configuration is minimal [Fig. 5(c), the leftmost part of the red curve]. When L_p exceeds $L_2 \approx 3.4$ nm, it becomes energetically favorable for the cylindrical TMD to distribute into the L_o phase since the hydrophobic mismatch between the TMD and the L_o bilayer becomes smaller than that between the TMD and L_d bilayer. However, as L_p increases, the energy of the TMD-induced deformations grows more steeply in the L_o phase as compared to the L_d phase, because the elastic moduli of the L_o bilayer are higher. At $L_p = L_4 \approx 5$ nm it again becomes energetically favorable for the cylindrical TMD to distribute into the L_d phase: although the TMD has a larger hydrophobic mismatch with the L_d bilayer, its compensation at the expense of the tilt [Fig. 5(d)] requires smaller energy since the L_d bilayer is substantially softer as compared to the L_o membrane.

The tilt degree of TMD is a function of its length. The TMD tilts substantially when its length exceeds the bilayer hydrophobic thickness by about 1 nm: $L_1 \approx 2h + 1\,\text{nm} = 4\,\text{nm}$ for L_d bilayer, $L_3 \approx 2h_o + 1\,\text{nm} = 4.6\,\text{nm}$ for the L_o bilayer [Fig. 5(d)]. Note that the characteristic lengths L_2, L_4 of the TMD transition between the phases are not directly related to the lengths L_1 and L_3 [Fig. 5(d)]. Dashed curves in Fig. 5(c) illustrate the dependences of the elastic energy of the membrane on the TMD length, $W(L_p)$, for the fixed zero tilt of the cylindrical TMD ($l = 0$). Qualitatively, the dependences are similar to those obtained for the optimized tilt, $W_0(L_p)$: there are also two characteristic lengths of the TMD lengths at which the energies of the deformations induced by the TMD in L_d and L_o bilayers coincide. However, quantitatively, the characteristic length $L_4^q \approx 5.6$ nm, the exceedance of which drives the TMD preferential distribution to the L_d phase at the zero tilt, is larger than $L_4 \approx 5$ nm [Fig. 5(c)].

Note that at characteristic lengths L_2, L_4 the energies of deformations induced by the TMD in the L_d and regular L_o phases are equal. This means that TMDs of such lengths should be equally distributed between the phases. However, the deviation of the TMD length from the characteristic one should lead to exponentially growing asymmetry of the TMD distribution between the phases, in accordance with the Boltzmann relation.

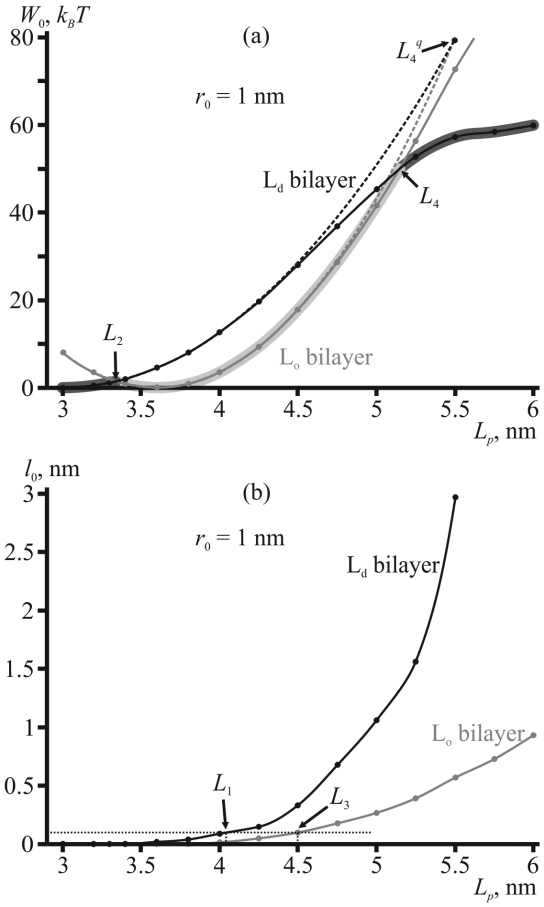

FIG. 6. Characteristic lengths of the cylindrical TMD weakly depend on its diameter. (a) The dependence of the membrane elastic energy in the configurations of optimally tilted TMDs W_0 on the TMD length L_p in the L_d bilayer (black curve) and regular L_o bilayer (gray curve). The curves intersect at two characteristic lengths $L_2 \approx 3$ nm and $L_4 \approx 5.1$ nm. Dashed curves illustrate analogous dependences for the zero tilt ($l = 0$); they intersect at $L_4^q \approx 5.5$ nm. Wide dark gray and light gray stripes indicate the membrane phase of the lowest energy. (b) The dependence of the optimal lateral shift of the TMD upper edge center on the TMD length. The dotted horizontal line corresponds to $l_0 = 0.1$ nm, which is arbitrarily chosen to represent the minimal substantial tilt. The intersections of the dotted line with the dependences $l_0(L_p)$ yield characteristic lengths of the TMD tilting: $L_1 \approx 4$ nm, $L_3 \approx 4.5$ nm in L_d and regular L_o bilayers, respectively.

B. Dependence of characteristic lengths on TMD diameter

To analyze possible dependences of TMD characteristic lengths on its diameter, we considered the case of the cylindrical TMD of the radius $r_0 = 1$ nm. The dependence of the elastic energy of L_d and regular L_o membranes optimized with respect to the TMD tilt on TMD length, $W_0(L_p)$, is shown in Fig. 6(a) for $r_0 = 1$ nm. Qualitatively, the dependences are quite similar to those in the case of $r_0 = 0.65$ nm [compare with Fig. 5(a)].

When the length of the cylindrical TMD matches the hydrophobic thickness of the bilayer, the elastic energy is zero ($L_p = 2h = 3$ nm for L_d and $L_p = 2h_o = 3.6$ nm for L_o bilayers, respectively). However, due to the larger TMD radius, the elastic energy grows more rapidly both in L_d and L_o membranes in the case of $r_0 = 1$ nm as compared to the case of $r_0 = 0.65$ nm. Nevertheless, the characteristic lengths of the TMD appear to depend on the TMD radius very weakly. In the case of $r_0 = 1$ nm, the characteristic lengths L_1 and L_2 are the same, while L_3 and L_4 changed only by about 0.1 nm, as compared to the case of $r_0 = 0.65$ nm: $L_1 \approx 3.3$nm, $L_2 \approx 4$ nm, $L_3 \approx 4.5$ nm vs 4.6 nm, $L_4 \approx 5.1$ nm vs 5 nm (Fig. 6). Almost equal lengths L_1 and L_3 mean that the characteristic length of the TMD controlling its tilt is mainly determined by the elastic properties of the membrane, while the detailed geometry of the TMD cross section is of less importance.

C. Dependence of characteristic lengths on elastic parameters of L_o phase

The elastic moduli of the L_o phase are not exactly known; moreover, they can vary depending on the particular composition of the membrane [21,22]. We analyzed the dependence of the TMD characteristic lengths on the rigidity of the L_o bilayer. The softest L_o bilayer considered (denoted by index e) has the same elastic moduli as the L_d membrane; the only difference is the larger hydrophobic thickness of the bilayer. The most rigid L_o phase (denoted by index f) is characterized by the five times higher bending modulus (as well as by the higher Gaussian and twist moduli, as they are directly related to the bending modulus in our model) and 10 times higher modulus of the lateral stretching. Additionally, three cases of the L_o bilayer of intermediate rigidity were considered; they are denoted by indices a, b, and r, from softer to more rigid, respectively. Optimized with respect to the TMD tilt, the dependences of the elastic energy of L_o membranes at different rigidities on the TMD length, $W_0(L_p)$, are shown in Fig. 7(a). The analogous dependence for the L_d bilayer is shown for comparison [red curve, Fig. 7(a)]. From the plot it follows that the characteristic length $L_p = L_2$ at which the elastic energies induced by cylindrical TMD in L_d and L_o membranes coincide and the condition $2h < L_p < 2h_o$ is fulfilled, changes only by about 0.1 nm as the L_o phase rigidity varies from the softest e to the most rigid f. However, the TMD characteristic length $L_p = L_4$ strongly depends on the L_o membrane rigidity: for the most rigid bilayer f $L_4 \approx 4.9$ nm, and L_4 gradually increases as the L_o phase becomes softer ($L_4^f < L_4^r < L_4^b < L_4^a$); finally, for the softest membrane e the elastic energies induced by the TMD in L_d and L_o bilayers never coincide [see orange and red curves in Fig. 7(a)].

The dependences $W_0(L_p)$ are very close to each other for the "firm" and "regular" L_o membrane; besides, $L_4^f \approx L_4^r$ [compare blue and green curves in Fig. 7(a)]. These membranes have equal bending moduli, $B_f = B_r = 5B$ (per monolayer), and two times different moduli of the lateral stretching, $K_a^f = 2K_a^r = 10K_a$. However, the dependences $W_0(L_p)$ for the "regular" and "soft-bending" cases differ substantially (in particular, L_4^r is less than L_4^b by about 0.5 nm), although these L_o bilayers have equal moduli of the lateral stretching ($K_a^r = K_a^b = 5K_a$) and 2.5 times different moduli of bending ($B_r = 2.5B_b = 5B$) [compare green and dark blue curves, Fig. 7(a)]. This allows concluding that the energy of elastic deformations induced by the TMD mostly depends on the bending modulus of the membrane, while the dependence on the modulus of the lateral stretching is minor. Indeed, the further decrease of the lateral stretching modulus by five times (i.e., transition from the "soft-bending" to "soft bending and stretching" cases) shifts the characteristic length L_4 by 0.25 nm only [compare dark blue and magenta curves in Fig. 7(a)].

The dependences of the optimal lateral shift of the TMD upper edge l_0 on L_p are shown in Fig. 7(b) for L_o bilayers of various rigidities. The characteristic length of the TMD tilting in the L_o bilayer L_3 depends on the bilayer rigidity: the softer the bilayer, the larger L_3, i.e., $L_3^f < L_3^r < L_3^b < L_3^a < L_3^e$ [Fig. 7(b)]. However, the dependence is quite weak: L_3 values for all considered cases of L_o phase rigidities fall into a relatively narrow range of 4.5–4.8 nm [compare blue and orange curves in Fig. 7(b)]. This allows concluding that the characteristic length of the TMD tilting is mainly determined by the hydrophobic thickness of the bilayer, while the elastic rigidity of the membrane has a minor effect.

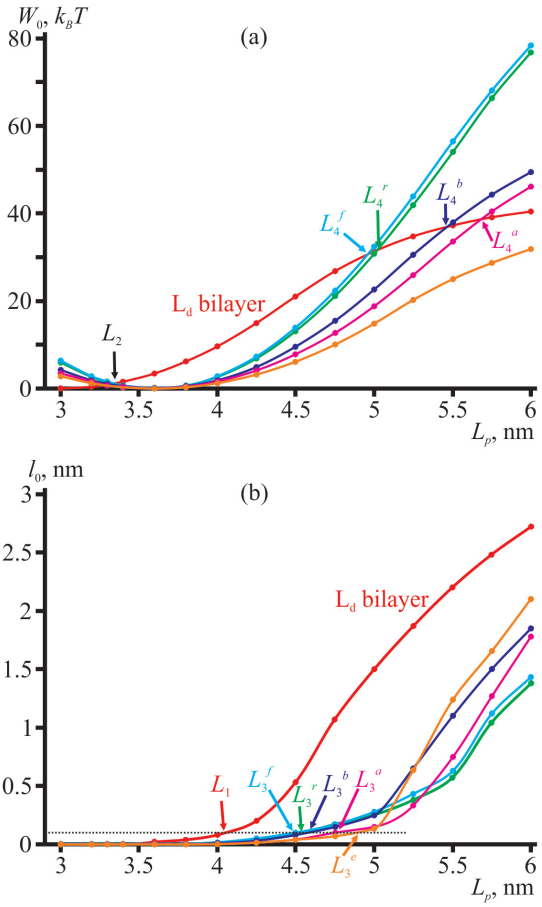

FIG. 7. Characteristic lengths of the cylindrical TMD, L_3 and L_4, strongly depend on the L_o bilayer rigidity. (a) The dependences of the membrane elastic energy in configurations of optimally tilted TMDs W_0 on the TMD length L_p in L_o bilayers of different rigidities: "firm" (blue curve), "regular" (green curve), "soft-bending" (dark blue curve), "soft bending and stretching" (magenta curve), and "very soft" (orange curve). The analogous dependence for the L_d bilayer (red curve) is shown for comparison. (b) The dependence of the optimal lateral shift of the TMD upper edge center on the TMD length. The dotted horizontal line corresponds to $l_0 = 0.1$ nm, which is arbitrarily chosen to represent the minimal substantial tilt. The intersections of the dotted line with dependences $l_0(L_p)$ yield characteristic lengths of the TMD tilting in the L_d bilayer ($L_1 \approx 4$ nm), and L_o bilayers of various rigidities ($L_3^f \approx 4.5$ nm, $L_3^r \approx 4.6$ nm, $L_3^b \approx 4.6$ nm, $L_3^a \approx 4.7$ nm, $L_3^e \approx 4.8$ nm).

D. Hourglass-like and barrel-like TMD

The dependences of $W_0(L_p)$ for the slightly hourglass-like (the normal component of the boundary director $n_n = -0.1$) and barrel-like ($n_n = +0.1$) shaped TMD are shown in Figs. 8(a) and 8(b). The analogous dependences for the substantially noncylindrical TMD ($n_n = \pm 0.5$) are shown in Figs. 8(c) and 8(d). In the case of the noncylindrically shaped TMD, the membrane elastic energy depends on the sponta-

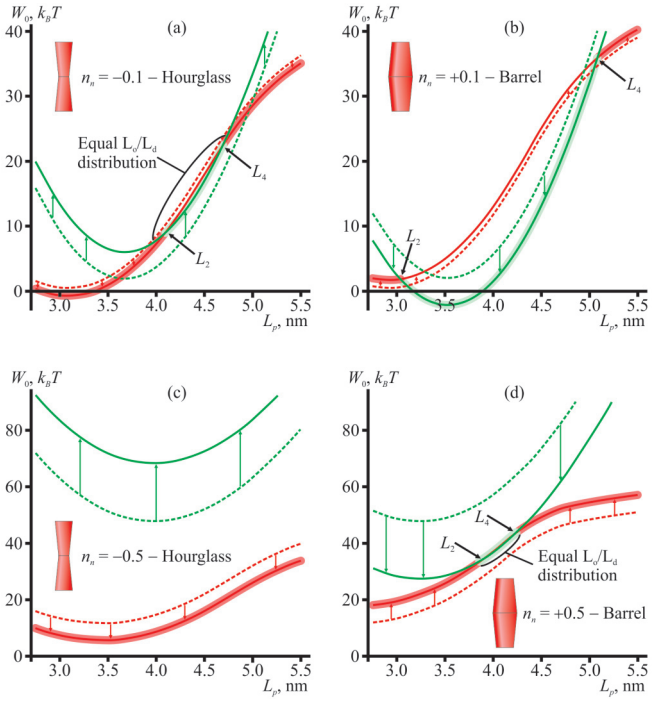

FIG. 8. Characteristic lengths of the hourglass-like (a), (c) and barrel-like (b), (d) TMD controlling its lateral distribution between L_d and L_o phases in the case when the deviation of the TMD shape from the cylinder is relatively small, $n_n = \pm 0.1$ (a), (b) or large, $n_n = \pm 0.5$ (c), (d). The dependence of the membrane elastic energy in the configurations of optimally tilted TMDs, W_0, on the TMD length, L_p, in the L_d bilayer (red solid curves) and regular L_o bilayer (green solid curves). Intersections of the curves determine two characteristic lengths L_2, L_4. Wide pink and light green stripes indicate the membrane phase of the lowest energy. Dashed curves illustrate analogous dependences for zero spontaneous curvatures of L_o and L_d phase monolayers ($J_0^r = J_0^s = 0$). The nonzero spontaneous curvature of the monolayer leads to the vertical shift (green and red vertical arrows) of the dashed curves by the constants, which are determined by Eq. (10).

neous curvature of its constituent monolayers [see Eq. (10)]. The corresponding contribution is constant and independent of the TMD length and tilt angle. The constant is proportional to the spontaneous curvature and bending modulus, and thus it is substantially different in L_o and L_d phases. The dependences $W_0(L_p)$ for the case of zero spontaneous curvatures of the membrane monolayers (i.e., ${J_0}^r = J_0^s = 0$) are shown in Fig. 8 as dashed curves. As the spontaneous curvatures of L_o and L_d monolayers have opposite signs, the dependences $W_0(L_p)$ shift in opposite directions for L_o and L_d phases if the spontaneous curvatures ($J_0^r = +0.1\,\mathrm{nm}^{-1}, J_0^s = -0.15\,\mathrm{nm}^{-1}$) are taken into account. In particular, for the hourglass-like shaped TMD, the curves $W_0(L_p)$ for L_d and L_o phases shift downwards [red vertical arrows in Figs. 8(a) and 8(c)] and upwards [green vertical arrows in Figs. 8(a) and 8(c)], respectively. The hourglass-like TMD induces a positive curvature in each monolayer, i.e., favors locally convex shape of the monolayer surface. However, macroscopically, the membrane is flat, i.e., it has zero geometric curvature. Thus, in the L_o phase monolayer, which has the positive spontaneous curvature, the introduction of the positively curved hourglass-like TMD leads to the increase of the deviation of the positive spontaneous curvature from zero geometric curvature. This leads to the increase of the elastic energy of the L_o membrane, resulting in the upward shift of the curve $W_0(L_p)$ [green curves in Figs. 8(a) and 8(c)]. On the other hand, in the L_d phase monolayer, the spontaneous curvature is negative, and the introduction of the positively curved hourglass-like TMD leads to the local decrease of the deviation of the negative spontaneous curvature from the zero geometric one. This leads to the decrease of the elastic energy of the L_d membrane, resulting in the downward shift of the curve $W_0(L_p)$ [red curves in Figs. 8(a) and 8(c)].

For the cylindrically shaped TMD, the elastic energy induced by the peptide of the length $L_2 < L_p < L_4$ is lower in the L_o phase as compared to the L_d phase [Fig. 5(c)]. This is also the case for slightly noncylindrical TMD ($n_n = \pm 0.1$) and zero spontaneous curvatures of the phases ($J_0^r = J_0^s = 0$) [Fig. 8(a), dashed curves]. In the case of the slightly hourglass-like TMD ($n_n = -0.1$) and spontaneous curvatures of L_o and L_d phase monolayers having opposite signs ($J_0^r = +0.1\,\mathrm{nm}^{-1}, J_0^s = -0.15\,\mathrm{nm}^{-1}$) the dependencies $W_0(L_p)$ shift upwards for the L_o phase and downwards for the L_d phase [Fig. 8(a)]. Because of this, in the range $L_2 < L_p < L_4$, the dependencies $W_0(L_p)$ for L_o and L_d phases approach each other and may even almost coincide [Fig. 8(a)]. In this case, the distribution coefficient of the peptide between the phases should be close to one in the wide range of the peptide lengths, e.g., from $L_p = 4\,\mathrm{nm}$ to $L_p = 4.75\,\mathrm{nm}$ for parameters of Fig. 8(a). For strongly noncylindrical hourglass-like TMD ($n_n = -0.5$) the curves $W_0(L_p)$ for L_o and L_d phases do not intersect [Fig. 8(c)]. The introduction of the nonzero spontaneous curvatures of the phases leads to an even larger distance between the curves $W_0(L_p)$; in this case, the L_d phase is strongly preferable in the whole range of peptide lengths [Fig. 8(c)].

For the barrel-like TMD, the introduction of the spontaneous curvatures of the phases ($J_0^r = +0.1\,\mathrm{nm}^{-1}$, $J_0^s = -0.15\,\mathrm{nm}^{-1}$) leads to the shift of the dependences $W_0(L_p)$ for L_d and L_o phases upwards [red vertical arrows in Figs. 8(b) and 8(d)] and downwards [green vertical arrows in Figs. 8(b) and 8(d)], respectively. The barrel-like TMD induces negative curvature in each monolayer, i.e., favors locally concave shape of the monolayer surface. Thus, in the L_o phase monolayer, which has the positive spontaneous curvature, the introduction of the negatively curved barrel-like TMD leads to the local decrease of the deviation of the positive spontaneous curvature from zero geometric curvature. This leads to the decrease of the elastic energy of the L_o membrane, resulting in the downward shift of the curve $W_0(L_p)$ [green curves in Figs. 8(b) and 8(d)].

On the contrary, in the L_d phase monolayer, the spontaneous curvature is negative, and the introduction of the negatively curved barrel-like TMD leads to the local increase of the deviation of the negative spontaneous curvature from the zero geometric one. This leads to the increase of the elastic energy of the L_d membrane, resulting in the upward shift of the curve $W_0(L_p)$ [red curves in Figs. 8(b) and 8(d)]. For the strongly noncylindrical barrel-like TMD ($n_n = +0.5$), the curves $W_0(L_p)$ built for the case of $J_0^r = J_0^s = 0$ do not intersect [dashed curves in Fig. 8(d)]. Upon the introduction of the spontaneous curvature ($J_0^r = +0.1\,\mathrm{nm}^{-1}$, $J_0^s = -0.15\,\mathrm{nm}^{-1}$),

the curves $W_0(L_p)$ approach each other, which may lead to the intersection or coincidence of the curves in a finite range of the TMD lengths, e.g., from $L_p = 3.8$ nm to $L_p = 4.3$ nm for parameters of Fig. 8(d). In this range, the distribution coefficient of the peptide between the phases should be close to one.

IV. DISCUSSION

The hydrophobic mismatch is considered to be one of the major driving forces that control the lateral distribution of transmembrane proteins between coexisting L_d and L_o phases [6]. The long enough TMD is thought to induce deformations of the adjacent L_d bilayer; the amplitude (and the energy) of the deformations can be decreased upon the TMD distribution into a thicker bilayer of the L_o phase. The hydrophobic mismatch can be compensated by either stretching the membrane in the vicinity of the TMD or by tilting the TMD with respect to the normal to the membrane plane [58–61]. Modeling the TMD tilt in the framework of continuum theories of elasticity is challenging as the symmetry of the membrane with the incorporated and tilted TMD is low; this prevents the analytical minimization of the elastic energy functional. For similar low-symmetry systems, even approximate analytical solutions of the optimization problem are coupled with the use of a nontrivial mathematic apparatus [42]. The interaction of tilted peptides mediated by membrane elastic deformations has been considered in a number of works [40,41]. However, in these works, the tilt angle of the peptides with respect to the membrane plane was fixed by the application of an external torque. The models were developed for transmonolayer rather than transmembrane peptides; so no hydrophobic mismatch could arise in the considered systems [40,41].

In the present work, we utilized the continuum theory of elasticity of lipid membranes to develop a model that allowed consideration of the TMD tilt as a possible mechanism of compensation of the hydrophobic mismatch with lipid bilayers of various thicknesses and elastic rigidity. We obtained that it becomes favorable to tilt the cylindrical TMD if its length exceeds the bilayer hydrophobic thickness by about 0.5 nm, although the considerable tilting is manifested for the exceedance of about 1 nm [Figs. 5(d), 6(b), 7(b)]. This value appeared to be rather universal: it varied but slightly for the TMD of different diameters (1.3 and 2 nm), for bilayers of different hydrophobic thicknesses (3 nm and 3.6 nm), which are characterized by an order of magnitude varying elastic moduli (the bending modulus from 10 to 50 k_BT; the modulus of lateral stretching from 133 to 1330 mN/m).

In a series of works, the tilt of transmembrane peptides of various lengths incorporated into lipid bilayers of different thicknesses has been investigated by means of molecular dynamics (MD) [58,62,63]. The optimal tilt angle is determined from the umbrella sampling procedure. The results of our calculations are in qualitative agreement with the results of molecular dynamics. Generally, longer peptides exhibit larger tilt angles in the bilayer of fixed hydrophobic thickness. The range of angles that can be thermally accessed around the optimal tilt angle is quite wide (of the order of 20°) both in MD [58] and in our model. Indeed, for long enough peptides (e.g., $L_p = 4$–5 nm) the dependences $W(l)$ near the minima l_0 are almost flat [Fig. 5(a)], and the exceedance of the minimal value $W(l_0)$ by $\sim 1\, k_BT$ determines the range of l corresponding to the tilt angles $(2l/L_p)$ of the order of 20°. The characteristic scale of the energy of the peptide tilting obtained by means of MD is similar to that of our model. For example, MD predicts that the tilting of the peptide, the hydrophobic length of which is about 0.4 nm shorter than the hydrophobic thickness of the lipid bilayer, by 40° should require about $10\, k_BT$ [58]. In our model, similar tilting requires about $12\, k_BT$ [Fig. 5(a)].

However, the optimal tilt angles predicted by MD are somewhat larger than those following from the continuum modeling [58,62,63]. This difference is attributed to the entropic contribution to the free energy that favors increasing tilt angles as this allows a larger number of the peptide states. This part of the energy is shown to decrease rapidly when the tilt angle varies from 0 to about 10°. Further, the energy monotonously decreases although slower; the total decrease reaches about $7\, k_BT$ in the range of angles 0–40° [58]. It is the entropic contribution that makes favorable the tilt of peptides that are even shorter than the hydrophobic thickness of the bilayer [58]. Such a counterintuitive effect cannot be described in the framework of our continuum model. However, the results of the works [58,62,63] can be distorted to some extent by the probable interaction of tilted peptides with the boundaries of the simulation box. The modeled membrane consists of 72 [58,62] or 100 [63] lipid molecules that corresponds to the linear size of the square box of about 5 to 6 nm only. In our recent work [41], we have demonstrated that the membrane-mediated interaction between two tilted transmonolayer peptides is still appreciable at separations of about 10 nm; the interaction of the transmembrane peptides should be even stronger.

In general, the methods that determine the peptide tilt angle on shorter timescales (such as MD [58,62] or those based on fluorescence spectroscopy [59]) yield larger optimal tilt angles than the methods based on longer timescale techniques (such as ^{2}H nuclear magnetic resonance (NMR) [60]). The underestimation of the tilt angles is attributed to partial motional averaging on longer observation timescales. Such smaller tilt angles are in better correspondence with our results, most probably, as our continuum model operates with elastic parameters of the membrane that are usually measured on relatively long timescales of seconds or minutes [53,64]. At the same time, NMR-based experiments report complete compensation of the hydrophobic mismatch only at the expense of the peptide tilt [60]. The works utilizing short-timescale techniques observe adaptation (stretching or compression, i.e., deformation) of lipid molecules contacting with the peptide. Our model predicts the dependence of the optimal tilt angles on the elastic moduli of the membrane [Fig. 7(b)], and thus agrees better with the results obtained from short-timescale approaches [54,55] in this aspect.

The characteristic length L_2, at which the energies of elastic deformations induced by the TMD in L_d and L_o bilayers coincide, depends, although rather slightly, on the elastic parameters of the L_o phase [Fig. 7(a)]. The coincidence of the energies implies that the distribution coefficient of the TMD between the phases should be close to 1. The distribution coefficient between L_o and L_d phases of 1.1 has been obtained for the TMD of the single-pass transmembrane protein, tLAT,

in giant plasma membrane vesicles (GPMVs) [6]. The truncation of the hydrophobic part of the TMD by six amino acids (i.e., by about 0.9 nm) results in the distribution coefficient of 0.6. Assuming that the lateral distribution of tLAT obeys the Boltzmann relation, we obtain that the energy difference for wild-type tLAT in L_o and L_d phases should be about $\ln(1.1/0.6) \approx 0.6\,k_BT$ lower than for truncated tLAT. In our model, the cylindrical TMD of the length $L_p = L_2 \approx 3.4$ nm should equally distribute between the L_d and L_o phases, i.e., manifest the distribution coefficient of about 1 [Fig. 5(c)]. The truncation of such a TMD by 0.9 nm results in $L_p = 2.5$ nm. Extrapolation of the quadratic approximations of the elastic energies [dashed lines in Fig. 5(c)] to $L_p = 2.5$ nm yields the energy difference of $17\,k_BT$ between L_o and L_d phases for the cylindrical TMD, which is much greater than the value of $0.6\,k_BT$ predicted from distribution coefficients determined experimentally [6]. However, plasma membranes, as well as GPMVs, consist of about 100 different types of lipids. In such a multicomponent system, the hydrophobic mismatch between the TMD and the membrane can be compensated directly by deformations of the lipid bilayer. Alternatively, the TMD can recruit lipid molecules of appropriate hydrophobic length, thereby forming a ring of boundary lipids [65] or inducing a local phase transition, e.g., by wetting mechanism [43,44]. In this case, the lateral distribution of the TMD between L_d and L_o phases should be mainly determined (or, at least, modulated) by the preferences of its boundary lipids to the particular phase of the membrane, rather than by the TMD itself. The dependence of the distribution coefficient of the TMD surrounded by boundary lipids on the TMD length should be qualitatively the same: the longer the TMD, the larger the distribution coefficient towards the L_o phase. However, quantitatively, the layer of boundary lipids is expected to substantially suppress this dependence. We hypothesize that such suppression may result in a very weak dependence of the distribution coefficient of LAT and its mutants on the TMD length as observed experimentally [6]. This hypothesis is in agreement with the observation that in model giant unilamellar vesicles consisting of three major lipid components of the plasma membrane tLAT is excluded from the L_o phase [66].

Another possible way to explain the experimentally observed weak change of the L_o/L_d distribution coefficient of tLAT upon its truncation is to admit that the actual effective shape of tLAT is not a cylinder. According to our calculations, in the case of a slightly hourglass-like shape of the TMD, its distribution coefficient between L_o and L_d phases may be close to one in a wide range of TMD lengths; this effect is illustrated in Fig. 8(a). However, to achieve a quantitative agreement, such an explanation requires an additional assumption that the effective "deformational" length of the wild-type (untruncated) tLAT is quite large [about 4.75 nm for parameters of Fig. 8(a)], i.e., larger than the actual length determined from its helical secondary structure [6]. A similar conclusion that the effective "deformational" length of the peptide should be larger than its actual length was made in the work [67]. In this work, the free energy change upon transfer of gramicidin A (gA) dimer from thin dilauroylphosphatidylcholine (DLPC) to thicker dimiristoylphosphatidylcholine (DMPC) bilayer has been calculated using MD. The actual "crystallographic" length of gA dimer approximately fits the hydrophobic thickness of DLPC bilayer. Thus, the transfer to the thicker DMPC bilayer was expected to give rise to an increase of the elastic energy due to the hydrophobic mismatch. However, the calculated energy decreased by about $3.8\,k_BT$ in the course of the DLPC → DMPC transfer of gA dimer [67]. To achieve a quantitative agreement with the MD data, it appeared necessary to assume that the effective "deformational" length of the gA dimer is larger than its "crystallographic" length by about 0.4 nm (i.e., by ∼20%) [67]. However, although the results and conclusions of the work [67] help a lot to justify the assumption of the large effective "deformational" length of the wild-type tLAT, which is necessary to explain the weak change of the L_o/L_d distribution coefficient of tLAT upon its truncation, we cannot exclude an alternative explanation of the MD data of this work. Indeed, it is implicitly assumed that the length of the gA dimer is the only parameter that determines the induced deformations in the membrane. However, the shape of the gA dimer is not strictly a cylinder, but rather an hourglass-like due to three relatively bulky tryptophan residues at C-terminal of each gA monomer, as visualized by means of MD in the works [45,46]. Thus, the membrane elastic energy induced by gA dimer is determined by both its length and the deviation of the dimer shape from the cylinder, i.e., by the normal component of the boundary director, n_n, in terms of our elastic model. To estimate the change of the elastic energy of the membrane upon DLPC → DMPC transfer of gA dimer, we utilized the following elastic parameters for DMPC (per monolayer): bending modulus $6.8\,k_BT$ [53]; hydrophobic thickness 1.275 nm [67]; lateral stretching modulus 117 mN/m [53]; tilt modulus 40 mN/m [48]; spontaneous curvature $+0.075\,\text{nm}^{-1}$ [68]. DLPC does not form stable bilayers, and to the best of our knowledge its elastic parameters are not determined. We can only roughly estimate the spontaneous curvature of DLPC monolayer as $+0.3\,\text{nm}^{-1}$. In the work [53] it is demonstrated that for DMPC and shorter lipid diC13:0 the lateral stretching and bending moduli are the same. Thus, for DLPC we used the values of the elastic moduli that are experimentally determined for DMPC. The hydrophobic thickness of the DLPC monolayer is 1.075 nm [67]. For the radius of the gA dimer we used the value of 1 nm, and we utilized its "crystallographic" length of 2.2 nm [67]. For such a set of the parameters, our model predicts the change of the elastic energy upon DLPC → DMPC transfer of gA dimer to be equal to $-3.5\,k_BT$, if the value of the normal component of the boundary director $n_n = -0.45$. This deviation of the gA dimer shape from the cylindrical one is quite large. We thus suppose that, most likely, both effects: (1) the increase of the effective "deformational" length as compared to the actual length and (2) the deviation of the gA dimer shape from the cylindrical one, should contribute to the determined value of the elastic energy change upon DLPC → DMPC transfer of gA dimer [67].

MD modeling of the lateral distribution of tLAT demonstrates its strong preference for the L_o/L_d phase boundary and somewhat weaker preference for the L_d phase: at the L_o/L_d phase boundary the energy of tLAT is about $4\,k_BT$ lower than in the L_d phase, while in the L_o phase the energy is about $11\,k_BT$ higher than in the L_d phase [69]. Such energy values are quite close to our calculated differences in energies of elastic deformations induced by the TMD incorporated into

the bulk of L_d and L_o bilayers. The preferential distribution of a transmembrane peptide to the L_o/L_d phase boundary, most probably, means that the hydrophobic length of the peptide is intermediate between hydrophobic thicknesses of L_d and L_o bilayers [30]. As demonstrated theoretically [24,25] and observed in MD modeling [55,56,70], there is a zone of a "hybrid" bilayer at the interphase boundary, the hydrophobic thickness of which is intermediate between that of L_d and L_o bilayers, $\sim(h + h_o)/2$. The zone is very narrow: its width is about 2–4 nm only [24,25,55,56,70]. Such a zone may provide conditions of minimal hydrophobic mismatch to the peptide. However, the capacitance of the "hybrid" zone to accommodate the peptides is finite. After its saturation, the peptides have to accumulate in the L_d phase, as demonstrated for tLAT by means of MD [69]. Besides, it is shown theoretically that a strong preference to the L_o/L_d phase boundary should have short ($L_p \sim 2h$) barrel-like peptides and long ($L_p \sim 2h_o$) hourglass-like peptides [36], i.e., the length of the peptide is not the only determinant of its lateral distribution. Note that when comparing the elastic energy of the peptides in the L_o and L_d phases we considered the bulk phases only. The bulk parts of the phases may differ from the boundary regions in local lipid composition, molecular packing, and, consequently, in elastic rigidities: the saturated lipids form rigid clusters that are bounded by the unsaturated lipids and cholesterol, as demonstrated by means of MD [71,72]. We took this inhomogeneity into account to some extent by attributing to the bulk L_o phase the values of the elastic moduli that substantially exceed those of the L_d phase. Although the L_o/L_d boundary region seems to be softer than the bulk L_o phase, its capacitance to accommodate the peptides is more limited than that of bulk L_o, L_d phases. Besides, modeling the tilted peptide at the L_o/L_d interphase boundary is quite challenging, because of low symmetry of such a system: all possible relative positions and orientations of the TMD and the boundary should be explicitly considered. In the future, such an analysis could be done in the framework of the model developed here.

The model peptide WALP23, the hydrophobic length of which is smaller than that of tLAT (17 vs 24 amino acids), is shown to accumulate in the L_d phase unless it is palmitoylated [73]. Palmitoylation drives WALP23 to the L_o-L_d phase boundary, while palmitoylated tLAT is shown to accumulate in the L_o phase [7]. Unfortunately, it is not obvious how to describe the case of palmitoylated peptides in the framework of our elastic model, as, most likely, the preference of the palmitic acid for the L_o phase has chemical rather than elastic nature. In the work [47] it was shown by means of MD that both WALP23 and longer transmembrane peptide WALP31 (TMD length 25 amino acids) prefer the L_d phase. In the course of the simulation, WALP31 demonstrated a strong tilt with respect to the membrane plane. In the case of artificially prevented tilt, WALP31 preferentially distributed to the L_o-L_d phase boundary. This may imply that the hydrophobic length of WALP31 has an intermediate value between the hydrophobic thicknesses of L_d and L_o bilayers and/or that its effective shape is not a cylinder, but rather an hourglass-like one.

At the characteristic length L_2 the energies of elastic deformations induced by the TMD in L_d and L_o bilayers are equal [Fig. 5(c)]. It seems that L_2 is close to the actual hydrophobic length of the longest transmembrane peptides studied experimentally or modeled by MD (e.g., tLAT, WALP31). For substantially (by 1.5–2 nm) longer cylindrical peptides or TMDs, our model predicts another characteristic length, L_4, at which the energies of elastic deformations induced by the peptide in L_d and L_o bilayers should coincide again [Fig. 5(c)]. This characteristic length is strongly dependent on the elastic parameters of the L_o bilayer [Fig. 7(a)] and dependent, although rather weakly, on the TMD diameter [Fig. 6(a)]. The origin of such a length is physically transparent. Long cylindrical TMDs should prefer to distribute to the L_o bilayer as this leads to the decrease of the hydrophobic mismatch. However, if the TMD length does not perfectly fit the hydrophobic thickness of the L_o bilayer, the TMD will induce elastic deformations in its vicinity. Since the L_o membrane is more rigid, with an increasing hydrophobic length of the TMD the energy of the deformations should grow up faster in the L_o membrane than in the L_d one even though, due to the larger hydrophobic thickness of the L_o membrane, the amplitude of the induced deformations is smaller. At the characteristic length of the TMD $L_p = L_4$, the energy of smaller elastic deformations arising in the more rigid L_o membrane matches the energy of larger deformations induced in the softer L_d bilayer. Longer TMDs, $L_p > L_4$, are thus predicted to prefer the L_d phase [Fig. 5(c), 7(a)]. As far as we know, such a regime has not been considered earlier. The strong dependence of the characteristic length L_4 on elastic properties of the L_o membrane may be used to experimentally determine the elastic moduli of the L_o phase, which are not exactly known to date.

The tilted transmembrane configuration of amphipathic α-helical peptides is demonstrated to be an intermediate stage of the pore formation process [74]. Such peptides are considered as perspective antimicrobial drugs. They are positively charged, which allows them to bind negatively charged outer leaflets of bacterial membranes [75]. At some critical surface concentration, the peptides transform from surface-bound to tilted transmembrane configuration to form a through pore in the bacterial membrane [74,76]. This process is cooperative, i.e., the pore is formed in the course of concerted action of several peptides. However, at the initial stage, the tilted transmembrane configuration is attained by a single peptide, as demonstrated by means of MD [74]. Although the probability of such a transformation is determined by the energy barrier rather than by the difference of the energies of the final (tilted transmembrane) and initial (surface-bound) states, the energy difference nevertheless represents estimation from below for the activation barrier. That is, the energy barrier cannot be lower than the difference of the energies of final and initial states. The elastic energy of the membrane in the surface-bound configuration of an amphipathic peptide can be obtained analytically in the framework of a unidimensional consideration, which has been shown to be quite accurate [35]. In the present work, we calculated the energy of elastic deformations induced by tilted transmembrane peptides in various conditions. Along with the results of the work [35], this provides a tool to estimate the probability of the initial stage of the pore formation by amphipathic peptides in membranes of different thicknesses, characterized by various elastic parameters. Such a tool may be useful for improving the selectivity of newly developed peptides, i.e., for better

binding to bacterial membranes and ignoring mammalian cell membranes.

In the present work, we calculated the energy of membrane deformations, which are induced by TMD in different configurations. The TMD was considered as a cylinder, hourglass-like or barrel-like rigid nondeformable membrane inclusion, which strictly imposes the boundary conditions on the adjacent lipids. However, the possibility of some influence of the surrounding bilayer on the TMD conformation cannot be excluded. In such a situation, the same TMD may impose different boundary conditions on the deformations, depending on what kind of a bilayer it is embedded in. Probably the simplest variant of such an adjustment is a change in the hydrophobic length of the TMD, which is likely accompanied by a simultaneous change in its diameter. The change in the diameter has a little effect on the characteristic lengths of the TMD (Fig. 6), while the influence of the length is quite strong; such an adjustment path thus seems possible and effective.

ACKNOWLEDGMENT

The work was supported by the Ministry of Science and Higher Education of Russia (Grant No. 075-15-2020-782).

[1] B. F. Lillemeier, J. R. Pfeiffer, Z. Surviladze, B. S. Wilson, and M. M. Davis, Proc. Natl. Acad. Sci. USA **103**, 18992 (2006).
[2] J. F. Frisz, H. A. Klitzing, K. Lou, I. D. Hutcheon, P. K. Weber, J. Zimmerberg, and M. L. Kraft, J. Biol. Chem. **288**, 16855 (2013).
[3] J. F. Frisz, K. Lou, H. A. Klitzing, W. P. Hanafin, V. Lizunov, R. L. Wilson, K. J. Carpenter, R. Kim, I. D. Hutcheon, J. Zimmerberg, P. K. Weber, and M. L. Kraft, Proc. Natl. Acad. Sci. USA **110**, E613 (2013).
[4] A. Pralle, P. Keller, E. L. Florin, K. Simons, and J. H. Hörber, J. Cell Biol. **148**, 997 (2000).
[5] L. J. Pike, J. Lip. Res. **47**, 1597 (2006).
[6] B. B. Diaz-Rohrer, K. R. Levental, K. Simons, and I. Levental, Proc. Natl. Acad. Sci. USA **111**, 8500 (2014).
[7] J. H. Lorent, B. Diaz-Rohrer, X. Lin, K. Spring, A. A. Gorfe, K. R. Levental, and I. Levental, Nat. Commun. **8**, 1219 (2017).
[8] M. Edidin, Trends Cell Biol. **11**, 492 (2001).
[9] K. Simons and E. Ikonen, Nature (London) **387**, 569 (1997).
[10] R. E. Brown, J. Cell Sci. **111**, 1 (1998).
[11] I. Levental, K. R. Levental, and F. A. Heberle, Trends Cell Biol. **30**, 341 (2020).
[12] S. L. Veatch, I. V. Polozov, K. Gawrisch, and S. L. Keller, Biophys. J. **86**, 2910 (2004).
[13] A. V. Samsonov, I. Mihalyov, and F. S. Cohen, Biophys. J. **81**, 1486 (2001).
[14] R. S. Petruzielo, F. A. Heberle, P. Drazba, J. Katsaras, and G. W. Feigenson, Biochim. Biophys. Acta **1828**, 1302 (2013).
[15] A. Saitov, S. A. Akimov, T. R. Galimzyanov, T. Glasnov, and P. Pohl, Phys. Rev. Lett. **124**, 108102 (2020).
[16] T. Baumgart, S. T. Hess, and W. W. Webb, Nature (London) **425**, 821 (2003).
[17] I. S. Vinklárek, L. Vel'as, P. Riegerová, K. Skála, I. Mikhalyov, N. Gretskaya, M. Hof, and R. Sachl, J. Phys. Chem. Lett. **10**, 2024 (2019).
[18] H. A. Rinia, M. M. Snel, J. P. van der Eerden, and B. de Kruijff, FEBS Lett. **501**, 92 (2001).
[19] A. J. García-Sáez, S. Chiantia, and P. Schwille, J. Biol. Chem. **282**, 33537 (2007).
[20] T. R. Galimzyanov, A. S. Lyushnyak, V. V. Aleksandrova, L. A. Shilova, I. I. Mikhalyov, I. M. Molotkovskaya, S. A. Akimov, and O. V. Batishchev, Langmuir **33**, 3517 (2017).
[21] T. Baumgart, S. Das, W. W. Webb, and J. T. Jenkins, Biophys. J. **89**, 1067 (2005).
[22] J. Pan, S. Tristram-Nagle, and J. F. Nagle, Phys. Rev. E **80**, 021931 (2009).
[23] P. I. Kuzmin, S. A. Akimov, Y. A. Chizmadzhev, J. Zimmerberg, and F. S. Cohen, Biophys. J. **88**, 1120 (2005).
[24] T. R. Galimzyanov, R. J. Molotkovsky, P. I. Kuzmin, and S. A. Akimov, Biol. Membrany **28**, 307 (2011).
[25] T. R. Galimzyanov, R. J. Molotkovsky, M. E. Bozdaganyan, F. S. Cohen, P. Pohl, and S. A. Akimov, Phys. Rev. Lett. **115**, 088101 (2015).
[26] L. P. Pitaevskii and E. M. Lifshitz, *Physical Kinetics*, Vol. 10 in Course of Theoretical Physics (Butterworth-Heinemann, Oxford, 2012).
[27] V. V. Slezov, J. Schmelzer, and Y. Y. Tkach, J. Phys. Chem. Solids **58**, 869 (1997).
[28] V. V. Slezov and J. Schmelzer, Phys. Rev. E **65**, 031506 (2002).
[29] V. A. J. Frolov, Y. A. Chizmadzhev, F. S. Cohen, and J. Zimmerberg, Biophys. J. **91**, 189 (2006).
[30] S. T. Yang, V. Kiessling, J. A. Simmons, J. M. White, and L. K. Tamm, Nat. Chem. Biol. **11**, 424 (2015).
[31] A. Y. Dunina-Barkovskaya and K. S. Vishnyakova, Biol. Membrany **37**, 381 (2020).
[32] A. Y. Dunina-Barkovskaya, K. S. Vishnyakova, L. A. Baratova, and V. A. Radyukhin, Biol. Membrany **36**, 271 (2019).
[33] J. H. Lorent and I. Levental, Chem. Phys. Lipids **192**, 23 (2015).
[34] I. Levental, D. Lingwood, M. Grzybek, U. Coskun, and K. Simons, Proc. Natl. Acad. Sci. USA **107**, 22050 (2010).
[35] O. V. Kondrashov, T. R. Galimzyanov, I. Jiménez-Munguía, O. V. Batishchev, and S. A. Akimov, Phys. Rev. E **99**, 022401 (2019).
[36] K. V. Pinigin, O. V. Kondrashov, I. Jiménez-Munguía, V. V. Alexandrova, O. V. Batishchev, T. R. Galimzyanov, and S. A. Akimov, Sci. Rep. **10**, 4087 (2020).
[37] G. Staneva, D. S. Osipenko, T. R. Galimzyanov, K. V. Pavlov, and S. A. Akimov, Langmuir **32**, 1591 (2016).
[38] O. V. Kondrashov, T. R. Galimzyanov, R. J. Molotkovsky, O. V. Batishchev, and S. A. Akimov, Membranes **10**, 368 (2020).
[39] K. Bohinc, V. Kralj-Iglič, and S. May, J. Chem. Phys. **119**, 7435 (2003).
[40] Y. Kozlovsky, J. Zimmerberg, and M. M. Kozlov, Biophys. J. **87**, 999 (2004).
[41] S. A. Akimov, O. V. Kondrashov, J. Zimmerberg, and O. V. Batishchev, Int. J. Mol. Sci. **21**, 5411 (2020).
[42] T. R. Weikl, M. M. Kozlov, and W. Helfrich, Phys. Rev. E **57**, 6988 (1998).

[43] S. A. Akimov, V. A. J. Frolov, P. I. Kuzmin, J. Zimmerberg, Y. A. Chizmadzhev, and F. S. Cohen, Phys. Rev. E **77**, 051901 (2008).
[44] R. J. Molotkovsky, T. R. Galimzyanov, O. V. Batishchev, and S. A. Akimov, Biomolecules **9**, 729 (2019).
[45] A. H. Beaven, A. M. Maer, A. J. Sodt, H. Rui, R. W. Pastor, O. S. Andersen, and W. Im, Biophys. J. **112**, 1185 (2017).
[46] T. Kim, K. I. Lee, P. Morris, R. W. Pastor, O. S. Andersen, and W. Im, Biophys. J. **102**, 1551 (2012).
[47] L. V. Schäfer, D. H. de Jong, A. Holt, A. J. Rzepiela, A. H. de Vries, B. Poolman, J. A. Killian, and S. J. Marrink, Proc. Natl. Acad. Sci. USA **108**, 1343 (2011).
[48] M. Hamm and M. M. Kozlov, Eur. Phys. J. E **3**, 323 (2000).
[49] S. Leikin, M. M. Kozlov, N. L. Fuller, and R. P. Rand, Biophys. J. **71**, 2623 (1996).
[50] P.-G. de Gennes and J. Prost, *The Physics of Liquid Crystals* (Oxford University Press, New York, 1995).
[51] O. V. Kondrashov, T. R. Galimzyanov, K. V. Pavlov, E. A. Kotova, Y. N. Antonenko, and S. A. Akimov, Biophys. J. **115**, 478 (2018).
[52] J. F. Nagle and D. A. Wilkinson, Biophys. J. **23**, 159 (1978).
[53] W. Rawicz, K. C. Olbrich, T. McIntosh, D. Needham, and E. Evans, Biophys. J. **79**, 328 (2000).
[54] M. Hu, D. H. de Jong, S. J. Marrink, and M. Deserno, Faraday Discuss. **161**, 365 (2013).
[55] H. J. Risselada and S. J. Marrink, Proc. Natl. Acad. Sci. USA **105**, 17367 (2008).
[56] J. D. Perlmutter and J. N. Sachs, J. Am. Chem. Soc. **133**, 6563 (2011).
[57] A. J. Sodt, R. M. Venable, E. Lyman, and R. W. Pastor, Phys. Rev. Lett. **117**, 138104 (2016).
[58] T. Kim and W. Im, Biophys. J. **99**, 175 (2010).
[59] A. Holt, R. B. Koehorst, T. Rutters-Meijneke, M. H. Gelb, D. T. Rijkers, M. A. Hemminga, and J. A. Killian, Biophys. J. **97**, 2258 (2009).
[60] E. Strandberg, S. Özdirekcan, D. T. Rijkers, P. C. van der Wel, R. E. Koeppe II, R. M. Liskamp, and J. A. Killian, Biophys. J. **86**, 3709 (2004).
[61] J. A. Killian, Biochim. Biophys. Acta **1376**, 401 (1998).
[62] J. Lee and W. Im, Phys. Rev. Lett. **100**, 018103 (2008).
[63] S. Özdirekcan, C. Etchebest, J. A. Killian, and P. F. Fuchs, J. Am. Chem. Soc. **129**, 15174 (2007).
[64] J. Genova, V. Vitkova, and I. Bivas, Phys. Rev. E **88**, 022707 (2013).
[65] P. C. Jost, O. H. Griffith, R. A. Capaldi, and G. Vanderkooi, Proc. Natl. Acad. Sci. USA **70**, 480 (1973).
[66] H. Shogomori, A. T. Hammond, A. G. Ostermeyer-Fay, D. J. Barr, G. W. Feigenson, E. London, and D. A. Brown, J. Biol. Chem. **280**, 18931 (2005).
[67] S. Park, M. S. Yeom, O. S. Andersen, R. W. Pastor, and W. Im, J. Chem. Theory Comput. **15**, 6491 (2019).
[68] S. A. Akimov, P. E. Volynsky, T. R. Galimzyanov, P. I. Kuzmin, K. V. Pavlov, and O. V. Batishchev, Sci. Rep. **7**, 1 (2017).
[69] X. Lin, A. A. Gorfe, and I. Levental, Biophys. J. **114**, 1936 (2018).
[70] D. A. Pantano, P. B. Moore, M. L. Klein, and D. E. Discher, Soft Matter **7**, 8182 (2011).
[71] A. J. Sodt, M. L. Sandar, K. Gawrisch, R. W. Pastor, and E. Lyman, J. Am. Chem. Soc. **136**, 725 (2014).
[72] A. J. Sodt, R. W. Pastor, and E. Lyman, Biophys. J. **109**, 948 (2015).
[73] D. H. de Jong, C. A. Lopez, and S. J. Marrink, Faraday Discuss. **161**, 347 (2013).
[74] K. P. Santo and M. L. Berkowitz, J. Phys. Chem B **116**, 3021 (2012).
[75] C. Pérez-Peinado, S. A. Dias, M. M. Domingues, A. H. Benfield, J. M. Freire, G. Rádis-Baptista, D. Gaspar, M. A. R. B. Castanho, D. J. Craik, S. T. Henriques, A. S. Veiga, and D. Andreu, J. Biol. Chem. **293**, 1536 (2018).
[76] J. Pan, D. P. Tieleman, J. F. Nagle, N. Kučerka, and S. Tristram-Nagle, Biochim. Biophys. Acta **1788**, 1387 (2009).